Journal of ELECTRONIC MATERIALS, Vol. 49, No. 1, 2020
https://doi.org/10.1007/s11664-019-07634-4
© 2019 The Minerals, Metals & Materials Society

TMS2019 MICROELECTRONIC PACKAGING, INTERCONNECT, AND PB-FREE SOLDER

Effect of Thermomigration–Electromigration Coupling on Mass Transport in Cu Thin Films

NALLA SOMAIAH[1] and PRAVEEN KUMAR[1,2]

1.—Department of Materials Engineering, Indian Institute of Science, Bangalore 560012, India.
2.—e-mail: praveenk@iisc.ac.in

Self-induced temperature gradients produced due to passage of electric current through thin film interconnects with bends can be very large, making thermomigration an important mass transport mechanism, in addition to electromigration. Here, we study effects of thermomigration–electromigration coupling on mass transport in Cu films deposited on SiO_2/Si substrate, as per the Blech configuration, with a W or Ta interlayer. We observed a slowly growing depletion zone at the anode in addition to a rapidly expanding depleted zone at the cathode. Moreover, we also observed that the extent of the depletion zone at the cathode varied non-monotonically with the inverse of the length of the sample. These seemingly "anomalous" observations are attributed to the coupling between thermomigration and electromigration, where thermomigration becomes dominant as the current density is increased, the sample length is decreased and the affinity between interlayer and the Cu film is weakened. The findings in this work are augmented by finite element modeling of thermomigration–electromigration coupling in Cu film. An overview of impact of these findings on fabrication of thin film device-level interconnects is also presented.

Key words: Blech length effect, Blech structure, Cu-Si thin film system, self-induced temperature gradient, thermomigration–electromigration coupling

INTRODUCTION

Modern microelectronic devices, advance micro- and nano-electrical mechanical systems (MEMS/NEMS), etc. comprise very narrow and very thin metallic interconnects, which carry currents of very high densities (e.g., $> 10^{10}$ A/m^2). In addition, continuous scaling down of devices and device systems has also led to a sharp decrease in the open spaces and packaging of dissimilar materials, including low-κ dielectrics that are often poor thermal conductors, in close proximity. An increase in the current density passing through thin metallic interconnects along with an increase in the electrical resistivity of the interconnects due to a large decrease in their dimensions, and poor thermal management have led to an increase in the operational temperature of these devices and device systems. The electric current of high densities (e.g., $> 10^8$ A/m^2), in the presence of relatively increased temperatures, is sufficient to drift the thermally excited ions in a metallic thin film interconnect. This mass transport is often termed as electromigration, which has been a major long-term reliability issue in microelectronic devices for the last several decades.[1–6] In addition, current crowding may occur at several locations in multi-level interconnects that are now commonly used in microelectronic devices and MEMS/NEMS. This is because when the electric current changes direction, e.g., when it moves from one arm of an angular interconnect to another arm (see Fig. 1a), or

(Received April 21, 2019; accepted September 11, 2019; published online September 23, 2019)

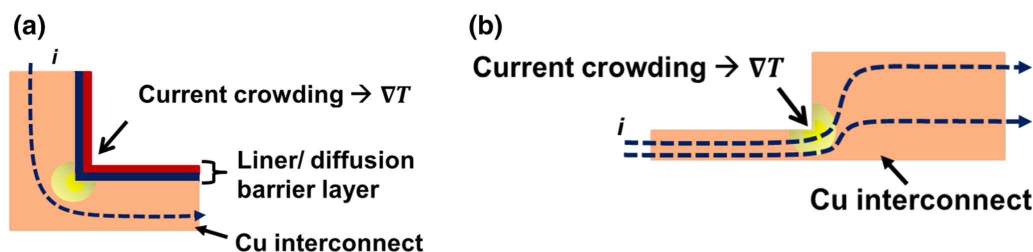

Fig. 1. Schematic illustration showing current crowding in thin Cu film interconnects with a (a) bend and (b) transition from a narrow region to a wider region.

changes magnitude, e.g., when it abruptly transitions from a narrow path into a wider path (see Fig. 1b) or encounters a cavity or a non-conducting inclusion, there is a change in the current density vector, which leads to current crowding at these transition locations or corners.[7,8] Since electromigration flux is proportional to the current density, the atoms at such locations experience much higher electromigration force than the atoms at other locations in the interconnect. Furthermore, due to the concentrated Joule heating caused by current crowding, the temperature at these locations will also be much higher than other locations in the interconnect. This makes the current crowding location "hot-spots" in the interconnect, which are the first to be damaged by electromigration.[7,9] In addition, formation of hot-spots establishes spontaneously a non-uniform distribution of temperature field in their vicinity. A non-uniform temperature field is marked by the existence of a temperature gradient, which can be as high as 10^5 K/m in the thin film interconnects with bends and junctions. In practice, this high temperature gradient can induce mass transport in thin film interconnects due to thermomigration.[10–14] Now, the presence of both thermomigration and electromigration may further exacerbate the overall mass transport in thin film device-level interconnects with locations of current crowding. This, therefore, necessitates the study of the effect of coupling between electromigration and thermomigration on the resultant mass transport in metallic films.

Interestingly, both electromigration and thermomigration are diffusion-controlled directional mass transport phenomena. Electromigration in solid metals commonly used as device-level interconnects, such as Cu or Al, results in mass transport from the cathode to the anode,[3,4] whereas thermomigration in these metals transports matter from the hot region to the cooler region.[10] Hence, depending on the directions of the mass transport due to thermomigration and electromigration in a thin film interconnect, the net mass transport can be manipulated. For example, for the system shown in Fig. 1a thermomigration and electromigration induced mass transports will be added and subtracted to determine the net mass transport in the vertical and horizontal channels, respectively. This is because the thermomigration mass transport in Cu film is always away from the region of the highest temperature towards the regions with lower temperatures, i.e., from the inner corner of the bend towards the uniform-sectioned channels, whereas the electromigration mass transport is from the right end of the horizontal channel (i.e., cathode) to the top end of the vertical channel (i.e., anode) in Fig. 1a. On the other hand, this coupling will be significant only in the wider section in Fig. 1b, as in the narrower channel the electromigration driven mass transport will be much more dominant due to the significantly higher current density in this channel as compared to the wider channel. Hence, the effect of thermomigration–electromigration coupling on mass transport will depend also on the geometry and current flow design of the system. It is imperative that a quantitative analysis of the net mass transport due to electromigration and thermomigration coupling is performed and its impact on the integrity of the Cu-Si thin film system, which is commercially the most important thin film system, is ascertained before the actual impact of such a coupling on the reliability of thin film device-level interconnects can be fully accessed.

Recently, we reported occurrence of mass depletion at the anode in Cu films deposited on Si as per Blech configuration due to significant thermomigration–electromigration coupling at the ends of Cu film.[14–17] We showed that the mass transport due to thermomigration and electromigration can be linearly superimposed.[14,15] It should be noted that although thermomigration and electromigration are diffusion-controlled phenomenon, they are driven by temperature gradient and electric field, respectively. Since their driving forces do not interact with each other, they are independent phenomenon and their coupling should be linear. Hence, coupling between them will not change the mechanism of mass transport by thermomigration or electromigration. Accordingly, if the "opposing" mass flux from the anode to the center of the Cu film due to thermomigration exceeds the mass flux from the cathode to the anode due to electromigration, then there can be net mass depletion at the anode also.[14,15] In addition, we also observed an *inverse Blech length phenomenon*, wherein the size of the mass depletion zone at the cathode in Cu film linearly increased with the inverse of the length of samples, in a Cu-Si thin film system due to the significant thermomigration–electromigration

coupling.[16,17] Herein, we suggested that the forward mass transport at the cathode due to thermomigration increased more rapidly than the opposing mass transport due to the stress gradient (built up from the anode to the cathode) with decrease in the sample length. This resulted in a larger depletion zone at the cathode with a decrease in the sample length.[16] However, the role of the duration of a test on the evolution of the nature of the thermomigration–electromigration coupling induced mass transport at the anode and the cathode has never been discussed. For example, it is not known if the inverse Blech length phenomenon will also be observed if the tests were run for very long durations. In addition, a general unified treatment of the aforementioned two extraordinary effects of the thermomigration–electromigration coupling on the mass transport in metal thin films, with a resolving perspective on why these phenomena may not be discerned in all tests, is not available in the literature. Here, we address these two issues, and also provide a solution for designing robust thin film device-level interconnects that are resistant to these seemingly "anomalous" mass transport phenomena occurring due to significant coupling between thermomigration and electromigration.

DETAILS OF EXPERIMENTS AND FINITE ELEMENT ANALYSIS

Experimental Procedure

In this study, samples comprising thin Cu film, SiO_2/Si substrate and W or Ta interlayer were fabricated as per the Blech configuration (see Fig. 2a). As can be inferred from Fig. 2a, electric current transitions from the highly resistive W or Ta thin interlayer to the significantly more conducting Cu thin film at the left edge of the sample and vice versa at the right edge of the sample. Hence, significant current crowding occurs at both edges of the Cu film. Accordingly, current crowding-induced temperature gradients at the edges of the metal film may initiate thermomigration. Interestingly, this sample configuration may spontaneously produce a condition wherein thermomigration and electromigration fluxes in the Cu film will be added at one of the ends (e.g., at the cathode where both transport matter towards the center of the film) and subtracted at the other edge (e.g., at the anode where electromigration and thermomigration transport matter towards the anode and away from the anode towards the center of the film, respectively). Moreover, due to the symmetry of the sample geometry, the magnitudes of the thermomigration as well as electromigration fluxes at both edges will be equal, and hence, their estimation using the principle of linear superposition is possible.[14,15] Hence, testing samples fabricated using the Blech configuration, which is the most commonly used sample design for studying electromigration in metals,[18] to understand the thermomigration–electromigration coupling is ideal. It should also be noted that due to the spontaneous current crowding, and hence, generation of the self-induced temperature gradient in the samples fabricated as per the Blech configuration, it also closely mimics the formation of hot-spots in the thin film interconnects used in the microelectronic devices and MEMS/NEMS employing multilevel architecture.

An approximately 7-μm-wide W or Ta interlayer and Cu thin films were sequentially deposited using direct current (DC) magnetron sputtering without breaking the vacuum. The thicknesses of the interlayer (i.e., W or Ta) and the Cu films were 30 nm and 150 nm, respectively. For deposition of all metallic thin films, a DC magnetron power of 120 W and Ar pressure of 4×10^{-3} mbar were used. Prior to deposition of the interlayer, a 100 nm thick SiO_2 layer was thermally grown on a 500-μm-thick (100)-oriented Si wafer by heating the wafer for 45 min at 1100°C in a dry oxidation furnace. Once the Cu film was deposited, patterning of the photoresist using standard photolithography was performed to chemically etch away some portion of the continuous Cu film to create segmented stripes of various lengths, namely 10 μm, 20 μm, 50 μm, 100 μm and 200 μm; Fig. 2b schematically shows the sample comprising Cu stripes. Cu etching was performed by dipping the sample into 0.1 M ammonium persulfate.

Tests on the fabricated samples were performed by passing electric currents of nominal densities of either 2×10^{10} A/m^2 or 4×10^{10} A/m^2 at a base pressure of $\leq 5 \times 10^{-6}$ mbar. Here, the nominal current density, j_0, was calculated by dividing the total current passing through the sample by the product of the sum of the thicknesses of the interlayer and the Cu thin film and the width of the Cu film (i.e., 180 nm $\times$ 7 μm = 0.126 μm^2). The sample was kept on a substrate heater whose temperature was maintained at a constant 250°C throughout the duration of the test. Tests were performed until either a pre-set time was reached or the resistance of the 200-μm-long stripe increased by 20%. The resistance of the 200-μm-long stripe was monitored using the 4-probe method, wherein the voltage was measured using the leads fabricated at the end of this stripe (see Fig. 2c). It should be noted that an increase in the electrical resistance of the longest stripe (i.e., 200-μm-long stripe) by 20% does not imply an increase in the resistance of the entire sample by the same amount. As will be discussed later, often the smallest of the stripes sustained much more damage during this time, suggesting that their resistance must have increased by a significant amount. Following the experiments, the top surface of the sample, especially at the both the ends of the Cu stripes, was observed using a scanning electron microscope (SEM).

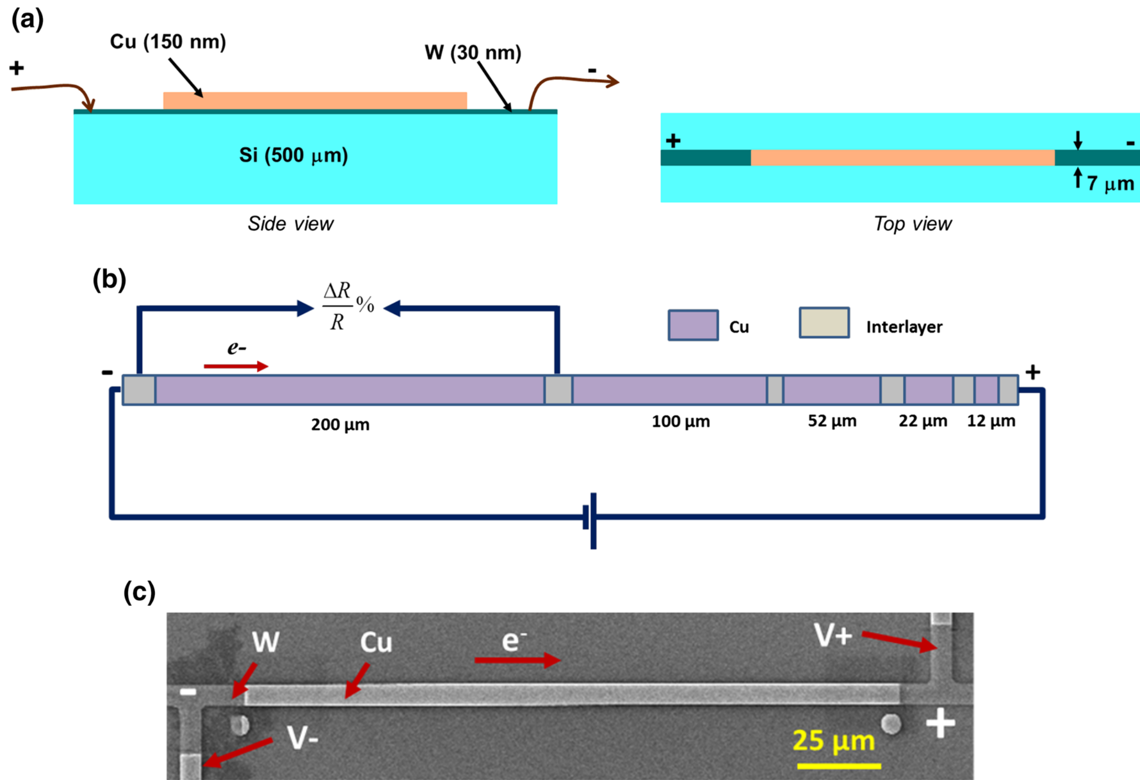

Fig. 2. Schematic illustration of (a) side view (left) and top view (right) of a thin film sample fabricated as per the Blech configuration and (b) the segmented sample comprising Cu stripes of various lengths used in this study. (c) SEM micrograph showing the top view of the 200 μm long stripe, along with the locations where the voltage was measured. Small circular pads near the ends of each Cu stripe were deposited to mark the initial boundaries of Cu stripe.

Details of Finite Element Analysis

Finite element analysis (FEA) was performed using COMSOL Multiphysics® to observe the effect of passing of an electric current, and the length of Cu stripes on the distribution of current density, temperature and temperature gradient in the sample to ascertain the role of the thermomigration in the mass transport in Cu films. Determination of temperature, temperature gradient and current densities in the Cu stripes, especially at their ends, allowed calculation of thermomigration–electromigration coupling in the samples, which could then be used to explain the experimental observations. Geometry of the 3D FEA model was prepared using the dimensions of the actual samples tested in experiments, and it was discretized using a 4-node tetrahedral element. Here, the effect of thickness on the electrical resistivity of metallic films was considered, wherein resistivity values of 7.7×10^{-8} Ω m, 14×10^{-8} Ω m and 2.2×10^{-8} Ω m were assigned to a 30-nm-thick W film, 30-nm-thick Ta film and 150-nm-thick Cu film, respectively.[19,20] SiO_2 and Si were assumed to be perfect insulators with infinitely high resistivity. For simplicity without compromising accuracy relevant for this study, thermal conductivities of all materials were assumed to be equal to the respective bulk values and all physical properties were assumed to be independent of temperature. Since the tests were performed in high vacuum, convection was not considered and heat loss only due to radiation was considered. The bottom surface of the Si substrate was maintained at substrate heater temperature, T_{SH}, of 250°C, whereas the ambient temperature was assumed to be equal to 25°C. Heat transfer in solids and electromagnetic heating physics modules of COMSOL Multiphysics® were employed to calculate the values of relevant parameters using FEA.

RESULTS AND DISCUSSION

"Anomalous" Mass Transport at the Anode: Observations and Effect of Test Duration

Figure 3 shows the top view of the regions near the cathode and the anode of a 100-μm-long Cu stripe in the Cu-Ta-SiO_2/Si sample before and after the completion of a test performed at T_{SH} = 250°C by passing an electric current of $j_0 = 2 \times 10^{10}$ A/m^2 for different durations. Here, Fig. 3a, b and c show both ends of the Cu stripe before the test, after a test that ran until the resistance of the 200-μm-long stripe increased by 20%, and after a test that ran for 125 h, respectively. It should be noted that the resistance of the 200-μm-long stripe increased by 20% just after ~ 20 h of the above test. A comparison of Fig. 3a and b reveals that the "regular"

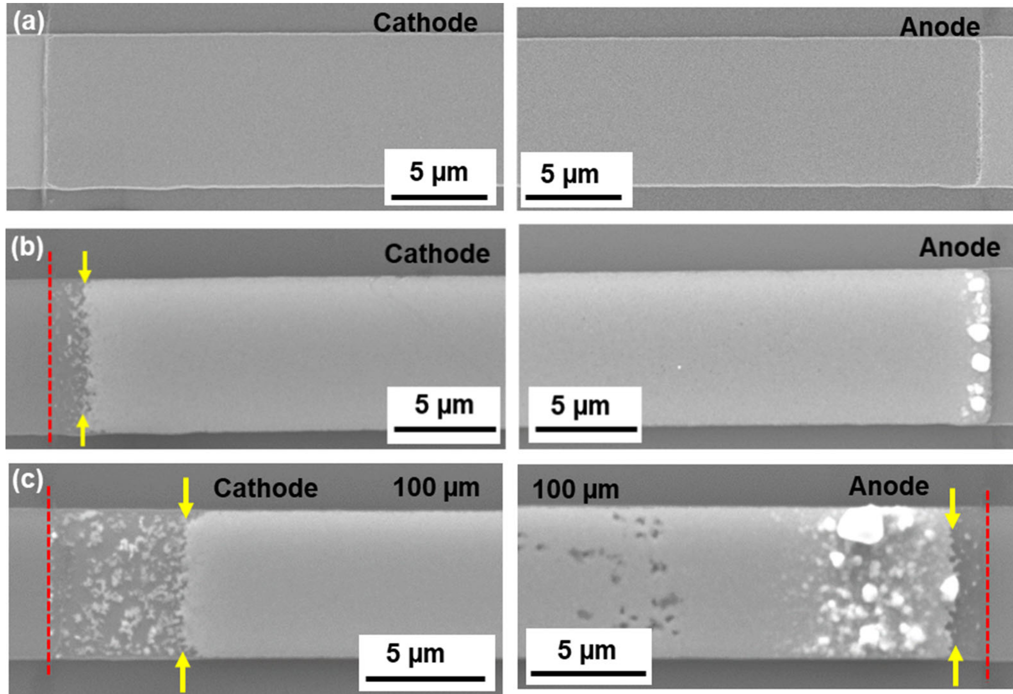

Fig. 3. SEM micrographs showing regions near the cathode (left panel) and the anode (right panel) of a 100-μm-long Cu stripe in a Cu-Ta-SiO_2/Si sample: (a) before the test, and (b) after a test performed until the resistance of the 200-μm-long stripe increased by 20%, and (c) 125 h. The test was performed at T_{SH} of 250°C by passing an electric current of $j_0 = 2.0 \times 10^{10}$ A/m^2. The broken (red) line shows the position of the edge of Cu film before the test, and the arrows (yellow) show the position of the corresponding edge after the test (Color figure online).

forward mass transport occurred from the cathode towards the anode, thereby forming voids at the cathode and hillocks near the anode. The extent of the depletion zone at the cathode (i.e., forward migration) in Fig. 3b was ~ 1.5 μm, while any mass depletion at the anode could not be discerned unambiguously at the magnification of micrographs shown in Fig. 3b. Interestingly, as shown in Fig. 3c, if the test was continued for longer duration of 125 h, then the mass depletion at the cathode increased considerably and a backward mass transport at the anode, resulting in mass depletion or void formation at the anode, could be observed in the sample. The formation of a depletion zone at the anode upon passage of electric current is considered *anomalous*, as it is unexpected under pure electromigration test condition.

For the test conditions shown in Fig. 3b and c, the average forward drift velocities, v_{fd}, calculated by dividing the extent of the depletion zone formed at the cathode by the total time, was equal to $\sim 1.9 \times 10^{-11}$ m/s and 1.7×10^{-11} m/s, respectively. These values of v_{fd} can be assumed to be the same, given the uncertainties in determining the location of the effective boundary of the depleted zone, and hence the drift at the cathode can be inferred to be occurring at constant rate throughout the test. The drift velocity of the backward mass transport measured at the anode, v_{bd}, using the micrographs shown in Fig. 3c and the procedure outlined above for calculating v_{fd}, was equal to $\sim 3.1 \times 10^{-12}$ m/s, which is substantially smaller than v_{fd}. If it is assumed that, similar to v_{fd}, v_{bd} also remained constant throughout the test, then the calculated v_{bd} using Fig. 3c would result in only a 0.2-μm-long depletion zone at the anode after 20 h (i.e., when the resistance of a 200-μm-long stripe increased by 20%, as shown in Fig. 3b). This depletion zone could not be resolved at low magnification and hence was not observed in Fig. 3b. Hence, although it appears from Fig. 3 that the anomalous backward mass transport at the anode initiates only after very long time, it may not be true.

In accordance to the observations made on Cu-Ta-SiO_2/Si samples, tests performed on Cu-W-SiO_2/Si samples also showed an enhanced forward mass transport at the cathode and the anomalous backward mass transport at the anode. An example set of micrographs showing regions near the cathode and the anode of the Cu-W-SiO_2/Si sample tested by passing an electric current of $j_0 = 2 \times 10^{10}$ A/m^2 at $T_{SH} = 250$°C (i.e., same test condition as for the Cu-Ta-SiO_2/Si sample shown in Fig. 3) is shown in Fig. 4. However, this test was stopped as soon as the resistance of the sample increased by 20%. Contrary to the Cu-Ta-SiO_2/Si sample, the Cu-W-SiO_2/Si sample showed unambiguously discernable anomalous mass transport at the anode by the time the resistance of the sample increased by 20%. A comparison of Figs. 3 and 4 also reveals that while the Cu film near the depleted zone at the cathode in

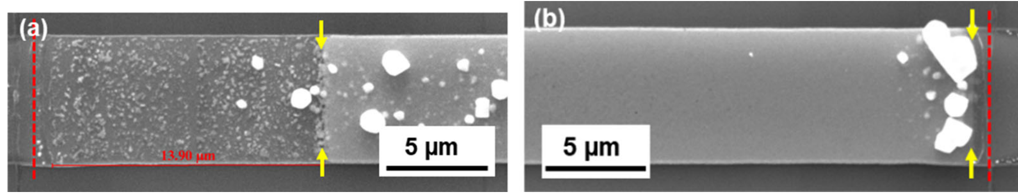

Fig. 4. SEM micrographs showing the top view of regions in the Cu-W-SiO_2/Si sample near the (a) cathode, (b) anode after a test performed at T_{SH} = 250°C by passing an electric current of $j_0 = 2.0 \times 10^{10}$ A/m^2 until the resistance of the 200 μm stripe increased by 20%. The line (red) shows the position of the Cu film before the test and the arrows (yellow) show the position of the respective edge of the Cu film after the test (Color figure online).

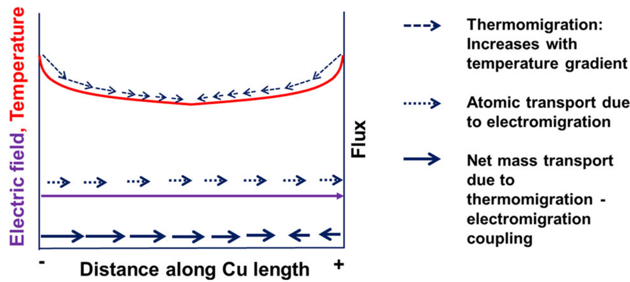

Fig. 5. A schematic illustration showing the (linear) superposition of electromigration- and thermomigration-induced mass transports, occurring during thermomigration–electromigration coupling. Here, the direction of the mass transport due to an stimulus is indicated by an arrow and the length of the arrow approximately show the relative magnitude of the rate of the mass transport.

the Cu-Ta-SiO_2/Si sample was free of hillocks, the same region in the Cu-W-SiO_2/Si sample had several small hillocks. Now, the extent of the depletion zones at the cathode and the anode in the Cu-W-SiO_2/Si sample were ~ 13.5 μm and 0.6 μm, respectively. These correspond to average v_{fd} and v_{bd} of 2.83×10^{-11} m/s and 1.24×10^{-12} m/s, respectively. This further confirms that v_{fd} and v_{bd} will be non-zero, but significantly different under these test conditions (i.e., when thermomigration–electromigration coupling is significant).

The above mass transport at the cathode and the anode can be understood by considering the superposition of the fluxes due to electromigration and thermomigration at these locations; this is schematically illustrated in Fig. 5. As shown in Fig. 5 (and will be shown later using FEA simulations), the highest driving force for thermomigration exists at both edges of the Cu films, such that Cu atoms at both edges of the film are pushed towards the center of the film by thermomigration. On the other hand, the mass transport due to electromigration throughout the Cu film remains unidirectional, from the cathode to the anode, and is reasonably constant. Hence, the backward mass transport at the anode occurred due to the dominance of the thermomigration-driven mass flux from the anode (i.e., high-temperature region) to the center of Cu film over the electromigration-driven mass flux from the cathode to the anode.[14,15] Now, given the slow rate of the backward mass transport in the tested samples, it becomes noticeable only after the forward mass depletion at the cathode has become quite significant. Hence, in an actual thin film device-level interconnect, the forward mass depletion at the cathode would have resulted in an open-circuit long before the backward mass transport at the anode would do the same. Hence, the forward mass transport at the cathode will remain the most crucial consideration in designing the interconnects. Nevertheless, the rate of the forward mass depletion is much faster under thermomigration–electromigration coupling condition than that under pure electromigration condition (see Fig. 5). Assuming linear superposition of the thermomigration and electromigration driving forces, which, as mentioned earlier, is reasonable, one can estimate the drift velocities due to pure electromigration, v_{EM}, and pure thermomigration, v_{TM}, in these tests. For example, v_{EM} and v_{TM} would be 7.5×10^{-12} m/s and 1.05×10^{-11} m/s, respectively, for tests performed using Cu-Ta-SiO_2/Si and 1.35×10^{-11} m/s and 1.48×10^{-11} m/s, respectively, for tests performed using Cu-W-SiO_2/Si samples. Hence, the rate of the mass depletion at the cathode, which first leads to the open-circuit of the thin film device-level interconnects, is more than double in case of thermomigration–electromigration coupling condition as compared to the pure electromigration condition (which is often considered while designing the thin film interconnects in current microelectronic devices).

Effect of Sample Length on Mass Transport

Figure 6 shows a few SEM micrographs of the cathode and anode ends of Cu stripes in a Cu-W-SiO_2/Si sample, which was tested by passing an electric current of $j_0 = 4 \times 10^{10}$ A/m^2 at T_{SH} = 250° C. As discussed in '"Anomalous" Mass Transport at Anode: Observations and Effect of Duration of Test' and as is evident from Fig. 6, both the forward mass transport at the cathode and the "anomalous" backward mass transport at the anode were observed at the end of the test on Cu-W-SiO_2/Si samples. As shown in Fig. 6, almost the entire volume of the material in 10-μm- and 20-μm-long stripes were transported into a small region; however, discernable backward and forward mass transports were observed in these stripes also. The extent of the depletion zone formed at both the cathode and the anode ends of all Cu stripes were

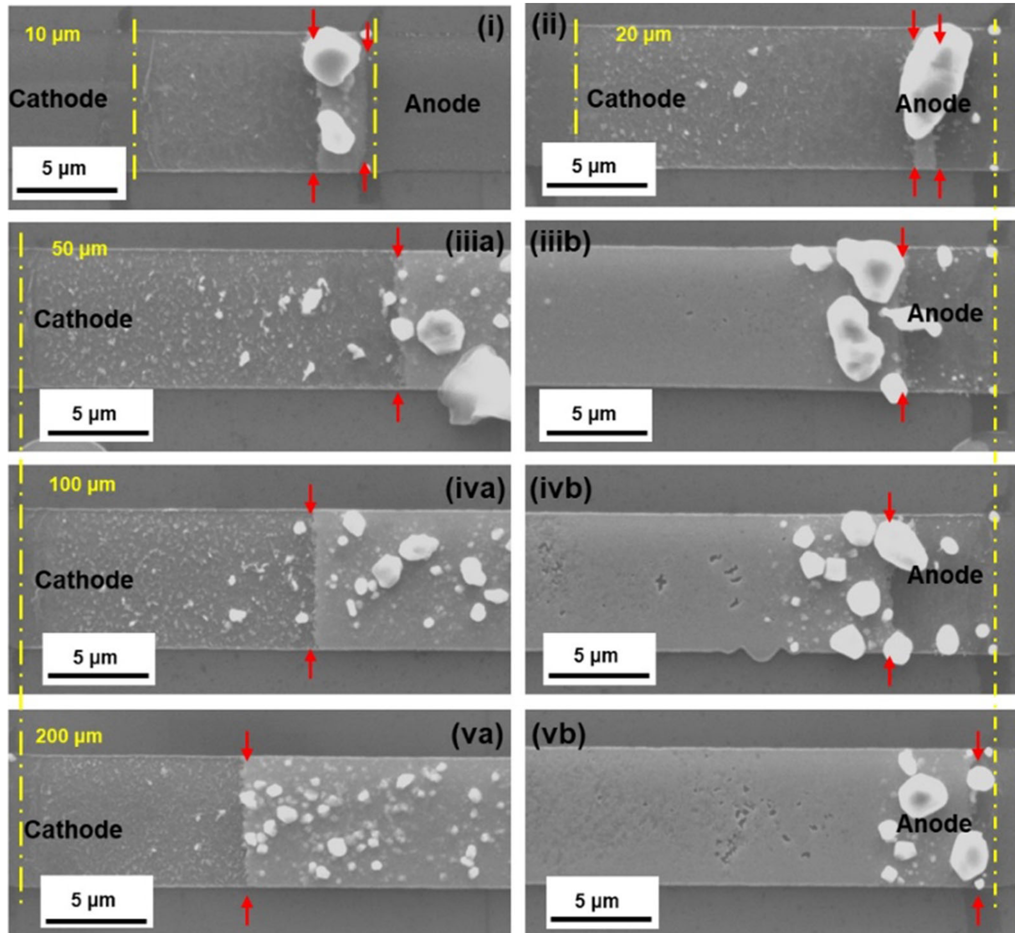

Fig. 6. SEM micrographs showing the regions near the anode and the cathode of stripes of various lengths, (i) 10, (ii) 20, (iii) 50, (iv) 100 and (iv) 200 μm, after the test performed at T_{SH} = 250°C by passing an electric current of $j_0 = 4 \times 10^{10}$ A/m^2. The line (yellow) shows the nominal position of the Cu edge before the test, and arrows (red) show the position of the same edge after the test. The test was terminated when the resistance of the 200-μm stripe increased by 20% (Color figure online).

measured and plotted against the inverse of the stripe length (see Fig. 7). As shown in Fig. 7, both forward and backward mass transport were non-monotonous functions of the inverse of sample length. As a matter of fact, a maximum in both types of mass transports was observed for the stripes of moderately long length (e.g., 50-μm- and 100-μm-long stripes, as indicated by point "B" in Fig. 7a and b, respectively) and the extent of the depletion zone decreased for both longer and shorter stripes.

Now, since the Blech length effect dictates a linear decrease in the forward mass transport at the cathode with the inverse of the sample length,[21–23] the observation shown in Fig. 7a (i.e., between points A and B) clearly suggests a deviation from the classic Blech length phenomenon in these samples. It should be noted that variation of the extent of the depletion zones formed at both the cathode and the anode with the inverse of stripe length can be represented, with reasonable confidence, by respective straight lines with negative slope in between points B and C in Fig. 7. Although this variation is similar to that dictated by the classic Blech length for the forward mass transport at the anode,* the variation between points A and B on both graphs in Fig. 7 is contrary to the classic Blech length. As a matter of fact, the existence of the backward mass transport at the anode warrants a change in the understanding of the classic Blech length, as both ends of the Cu film are not only depleted of atoms, but also a reserve of atoms in the form of hillocks are established in the vicinity of both depletion zones (see Fig. 6). Hence, the opposing stress gradient from the hillock region (which is deprived of vacancies) to the depleted region (which is richer in vacancies) is established only locally near both ends of the Cu stripe. Overall, Fig. 7 shows that not only the mass transport at both ends of Cu stripes was similar in these samples, but also the moderately long Cu stripes were invariably quite resistant to the mass transport at both the cathode and the anode. This further confirms that

*Blech length for the backward mass transport occurring at the anode has never been reported.

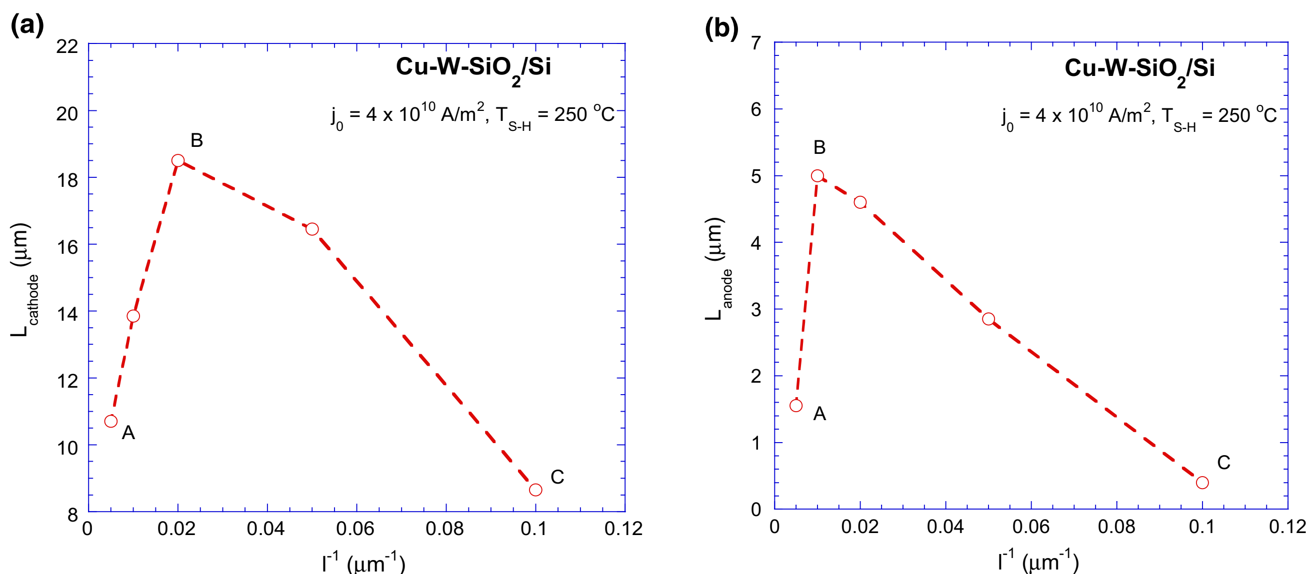

Fig. 7. Variation of the length of the depletion zone formed at the (a) cathode due to the forward mass transport and (b) anode due to the anomalous backward mass transport as a function of the inverse of the Cu stripe length. The data reported here correspond to the SEM micrographs shown in Fig. 6.

the thermomigration–electromigration coupling induced mass transport is fundamentally different from pure electromigration.

Now, as shown in Fig. 6i and ii, the shortest two Cu stripes shrunk to a very small length following the electric current loading. This casts doubt on the ability to do a meaningful measurement of the depletion zones at the cathode and the anode, as continuous undeterred mass transport in these stripes might not have occurred until the end of the test. Hence, running a test until the resistance of the 200-μm stripe increased by 20% is perhaps too long to measure a non-stagnant mass transport in the 10-μm and 20-μm stripes. To avoid this issue, samples were tested for a much shorter duration of only 30 min at the same j_0 of 4×10^{10} A/m^2 and T_{SH} of 250°C. Figure 8a shows SEM micrographs of the region of Cu stripes near the cathode after the test, which clearly reveals an increase in the extent of the depletion zone at the cathode with a decrease in the length of the Cu stripe. It should be noted that backward mass transport at the anode could not be discerned in this sample after this short-term test. Now, Fig. 8b clearly reveals a linear increase in the extent of the forward mass transport at the cathode with the inverse of the sample length. This behavior is contrary to the classical Blech length effect, and hence we term it the *inverse Blech length phenomenon*. A comparison of Figs. 7a and 8 suggests that the expanse of region AB in Fig. 7a decreases with increase in the duration of the test, i.e., as the length of the stripe is further decreased with continued testing. The reason for this mass transport behavior is not understood now; however, it may depend on the establishment of the modified stress gradient over a smaller length scale at each end of the Cu film because the backward mass transport became significant with an increase in the test duration (as hillocks started to form near ends of Cu film only after significant backward mass transport—see Fig. 6). In summary, a comparison of Figs. 7 and 8 clearly reveals that the occurrence of the classic or inverse Blech length effect will depend on the time duration of the tests, wherein chances of unambiguous observation of inverse Blech length will be high if the tests were performed for short duration. On the other hand, if the issue with measurement of the depletion zones in very short stripes is ignored, then the classic Blech length may *apparently* be observed in most stripes (except for the very long stripes) if the tests are performed for very long duration.

Role of Test Parameters on Thermomigration–Electromigration Coupling

In the two previous sections, the effect of thermomigration–electromigration coupling on mass transport in Cu-Si thin film systems was discussed. The reason for the occurrence of significant thermomigration is because high temperature gradients are spontaneously established at the ends of Cu films in Blech samples upon passage of an electric current of high density. This can be studied using FEA. Figure 9a and b, which shows the 2D color-coded temperature field near one of the edges of the Cu stripes in Cu-Ta-SiO_2/Si and Cu-W-SiO_2/Si samples, respectively, clearly reveal that distribution of temperature near the edges was non-uniform. Interestingly, FEA simulations reveal that the Cu film registered temperature gradients of as high as 10^6 K/m, especially near the interface of the interlayer and the Cu film, near its edge. To gain

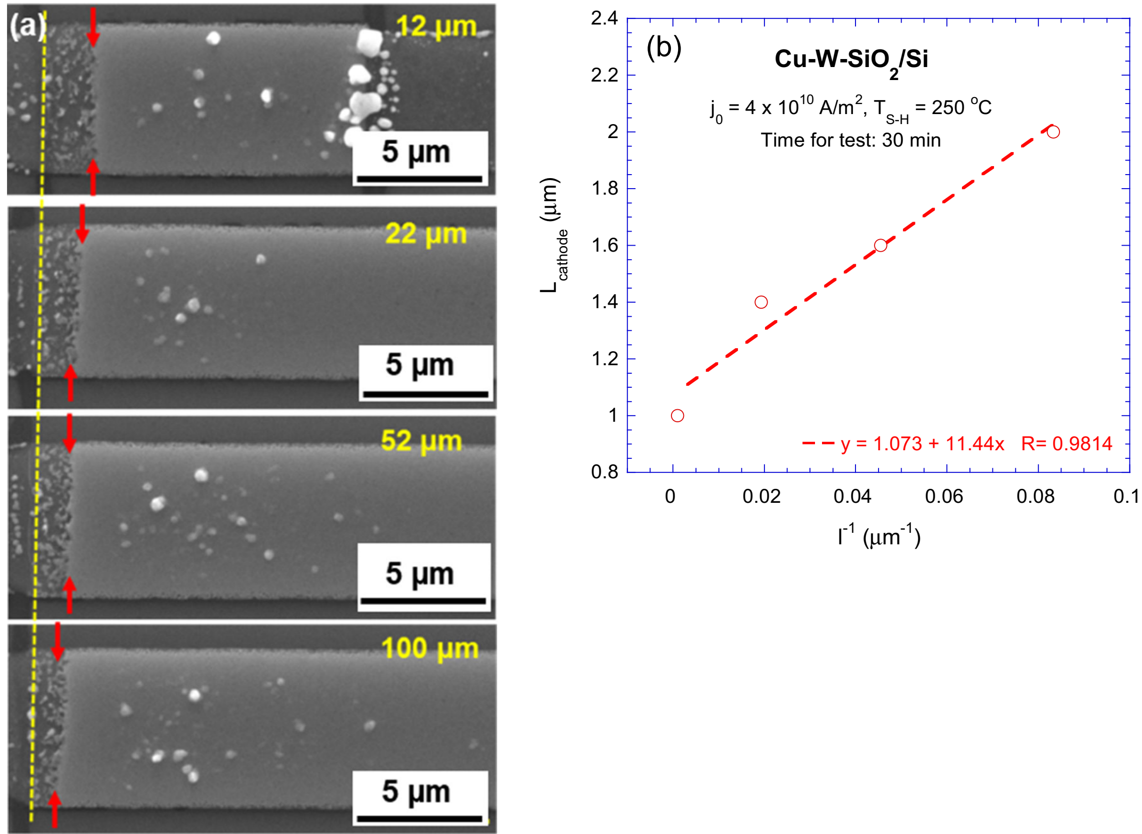

Fig. 8. (a) SEM micrographs of Cu stripes in a Cu-W-SiO_2/Si sample showing the depletion zone in the vicinity of the cathode. Test was performed by passing an electric current of $j_0 = 4 \times 10^{10}$ A/m^2 at $T_{S\text{-}H}$ = 250°C for 30 min. The broken (yellow) line shows the position of the Cu film before the test and the arrows (red) show the position of the respective edge of the Cu film after the test. (b) Variation of the extent of the depletion zone near the cathode (i.e., forward mass transport), as shown in (a), as function of inverse of the stripe length. The data in (b) was replotted from Fig. 4a of Ref. 16.

further insights into the nature of the variation of the temperature gradient in the Cu film, variation of the temperature gradient was plotted as a function of the distance away from the interface along the thickness of the Cu film (see Fig. 9c) and the distance away from the edge of the Cu stripe along the interface of the interlayer and the Cu film (see Fig. 9d). Figure 9c and d clearly reveal existence of the highest temperature gradient near the Cu-interlayer interface at the end of the Cu stripe (i.e., consistent with Fig. 9a and b). Figure 9d also reveals that the temperature gradient rapidly dropped away from the edge of the Cu film, reaching a saturated or minimum value at the center of the Cu stripe. Overall, Fig. 9 shows that the magnitude of the temperature gradients in Cu film is high enough to induce thermomigration from both ends of Cu film towards the center of the Cu film, especially along the interface between Cu and interlayer. Hence, the results obtained in the tests reported in the two previous sections are indeed affected by significant thermomigration–electromigration coupling.

A careful observation of Fig. 9 reveals that the temperature gradient and hence the driving force for the thermomigration (and thermomigration–electromigration coupling) in Cu-Ta-SiO_2/Si samples was higher than that in Cu-W-SiO_2/Si sample. In addition, since the electrical resistivity of Ta is significantly higher than that of W, the current density in Cu will be significantly higher in Cu-Ta-SiO_2/Si sample. Hence, the electromigration force will also be higher in the sample with Ta interlayer. However, v_{fd} for the sample with Ta interlayer was about two-thirds of that for the sample with the W interlayer. This apparent dichotomy can be explained by comparing the interfacial layers formed between Cu and W films and Cu and Ta films. As shown in Fig. 10, which shows high-resolution transmission electron micrographs with cross-sections of Cu-W and Cu-Ta interfacial layers, the interfacial layer formed between Cu and W was primarily amorphous, whereas the interfacial layer formed between Cu and Ta was partially crystalline. This is consistent with heat of mixing data, which shows stronger affinity between Cu and Ta, as compared to that between Cu and W. Now, it is reasonable to assume that diffusivity through generally more open amorphous interfacial layer (i.e., Cu-W) would be faster than that through a semi-crystalline interfacial layer (i.e., Cu-Ta), and hence the kinetics of mass transport in Cu-W interfacial layer would be faster.

Fig. 9. FEA simulation results showing the distribution (color-coded) of temperature gradient for (a) Cu-Ta-SiO_2/Si and (b) Cu-W-SiO_2/Si samples near one of the edges of a Cu stripe. Variation of temperature gradient along (c) thickness near the edge of Cu film and (d) distance away from the edge of Cu film near the interfacial layer. The data for Ta as shown in (c) and (d) are taken from Ref. 17. These FEA results justify the schematic illustration of temperature field in Fig. 5.

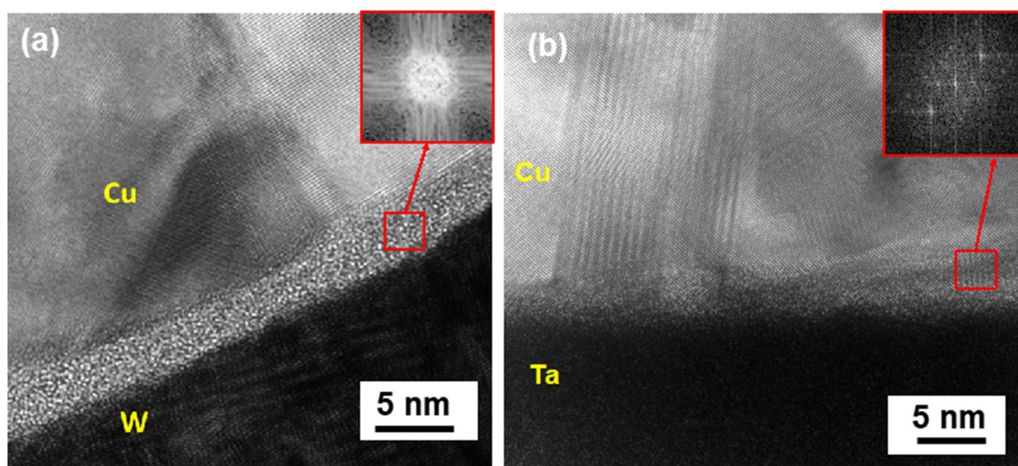

Fig. 10. High-resolution transmission electron micrographs showing the interfacial region formed between (a) Cu and W films and (b) Cu and Ta films. The inset shows fast Fourier transform from a representative region in the interfacial layer.

It should be noted that the kinetics of thermomigration–electromigration coupling is diffusion-controlled, which depends on the area of diffusion path and diffusivity through the path. Now, a diffusing Cu atom can go from one point to another via either lattice (which is often the slowest path at low temperatures), grain boundary, surface (which may have oxide layer and hence may not be practically

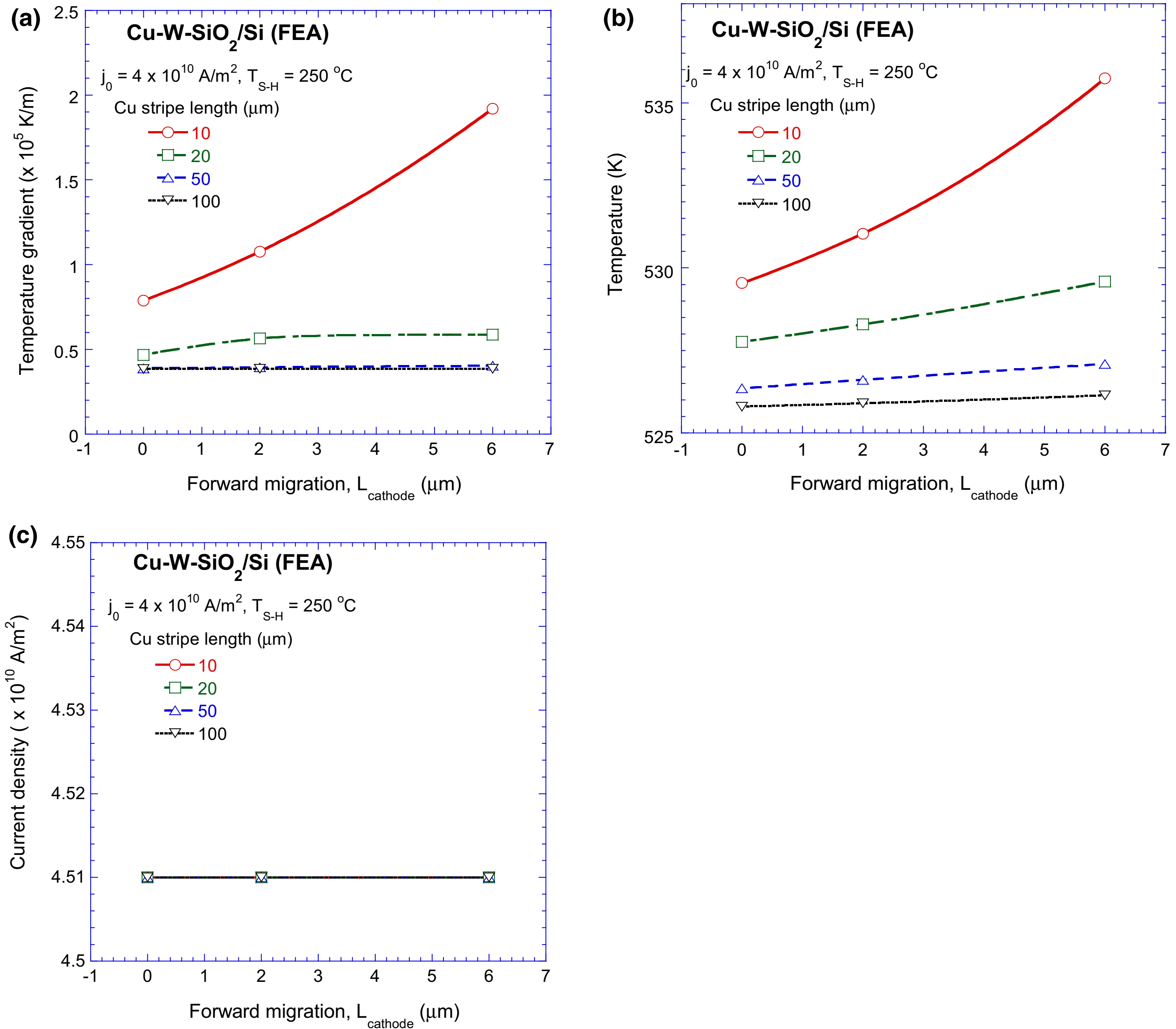

Fig. 11. FEA simulation results showing variation of (a) temperature gradient, (b) temperature and (c) current density near the center of the Cu stripes of various lengths as function of the forward migration at the cathode. These values, which also correspond to the minimum values of the parameters in a stripe, were estimated 0.1 nm above the interface between the interlayer and the Cu film. These FEA results justify the schematic illustration of electric field in Fig. 5.

very conducive for fast diffusion) or interface between film and the interlayer. When the interface between film and interlayer is weak (or open), its contribution in migrating the Cu atoms dominates those through the lattice (or bulk), grain boundary and top surface. Hence, even though the driving force for thermomigration (and hence thermomigration–electromigration coupling) is higher in the Cu-Ta-SiO_2/Si sample, the slower kinetics of mass transport through the interfacial layer formed between Cu and Ta results in a much slower drift rate and hence shorter depletion zone. It should be noted that irrespective of the interlayer, the highest driving force for the thermomigration, and hence thermomigration–electromigration coupling, exists at the interface between the interlayer and the Cu film (see Fig. 9), and hence diffusivity through the interfacial layer plays the dominant role in transporting required material. This suggests that placing an interlayer with strong affinity to Cu restricts the thermomigration–electromigration coupling induced unexpected mass transport.

To further understand the effect of thermomigration–electromigration coupling on the initial stages of mass transport occurring at the cathode (i.e., when the anomalous backward mass transport at the anode is not significant), FEA-based simulations were performed to predict the variations of temperature, temperature gradient and current density in the center of the stripe, wherein their values are the minimum (see Fig. 9d), as a function of stripe length and the forward migration. As shown in Fig. 11a,

the value of the minimum temperature gradient in the stripe increased with both a decrease in the stripe length and, consistently, an increase in the extent of the forward mass transport (which effectively makes the sample length smaller). Similarly, Fig. 11b shows that the minimum temperature in the Cu stripe also increased with the decrease in length of the sample and the increase in the forward mass transport. Interestingly, Fig. 11c does not show any significant effect of the stripe length and the forward mass transport on the minimum current density. Since the electric current (and its crowding at the edges) is responsible for the Joule heating, the observed effect of the sample length (as well as the forward mass transport) on the temperature and temperature gradient must originate from the fact that the proximity of the center of the sample to the edges of the Cu film, where current crowding occurs, increases with a decrease in the stripe length.

Since the temperature gradient, and hence the driving force for the thermomigration, increases rapidly with the decrease in the sample length without significant increase in the current density and hence electromigration driving force, it is reasonable to assume that the shorter samples will be increasingly more affected by the thermomigration induced mass transport. This will enhance the forward mass transport at the cathode. On the other hand, as the minimum (and hence overall) temperature of the sample increased with decrease in the sample length, it is reasonable to assume that the value of the opposing backward stress gradient, which often scales with the ratio of the compressive yield strength** of the material and the sample length, will not grow as rapidly with decrease in the sample length as in the case when the effect of sample length on the temperature is negligible (i.e., the ideal case of classic Blech length). Therefore, while the driving force for the forward mass transport increases rapidly with decrease in the sample length, the opposing backward stress gradient does not resist the mass transport in similarly increased fashion. This results in a net increase in the forward mass transport at the cathode with a decrease in the sample length. Hence, the variations of temperature gradient, temperature and current density with inverse of the sample length, as shown in Fig. 11, are responsible for the inverse Blech length phenomenon as discussed in 'Effect of Sample Length on Mass Transport'. Since the net effect of the decrease in the opposing backward stress gradient and the increase in the forward driving thermomigration force may not be a monotonic function of the inverse of the sample length, a maximum in the net forward mass transport at the cathode could be observed, as shown in Fig. 7a.

**Yield strength of most of the metals decreases with an increase in the temperature.

SUMMARY

Blech structure is quite suitable for studying thermomigration–electromigration coupling-induced mass transport in thin metallic films. An anomalous backward mass transport in Cu thin film was observed at the anode, which was unambiguously discerned if the tests were run for long durations. The forward mass transport at the cathode occurred at a much faster rate. The anomalous backward mass transport at the anode and the asymmetry in the drift velocities for forward and backward mass transport can be attributed to the thermomigration–electromigration coupling: while thermomigration and electromigration work in unison at the cathode, they oppose each other at the anode. To obtain anomalous backward mass transport at the anode, the thermomigration driving force must dominate the electromigration driving force.

The mass transport rate in Cu-Si sample with a W interlayer was faster than that with the Ta interlayer, even though the self-induced temperature gradient and the current density in the Cu film were higher in the sample with the Ta interlayer. This apparent dichotomy is attributed to the slower rate of diffusion through partially crystalline Cu-Ta interfacial region, as compared to the mostly amorphous Cu-W interfacial region. Using an interlayer with very strong affinity to Cu may suppress these unexpected mass transport phenomena.

If the tests were performed for short duration, the Cu-W-SiO_2/Si sample showed a linear increase in the forward mass transport at the cathode with inverse of the length of the Cu film, thereby showing *inverse Blech length phenomenon*. This was attributed to the rapid increase in the temperature gradient driven forward mass transport with the decrease in the sample length.

Since the described coupling between thermomigration and electromigration, which is inevitable in real multi-level interconnects, exacerbates the electric current driven damages in thin metallic films, this set of observations warrants a change in the philosophy for designing interconnects that are resistant to electric current induced damages.

ACKNOWLEDGMENTS

The authors would like to thank the Department of Science and Technology (DST), Government of India, for financial support (DSTO #1164 and #1526). The authors also thank Professor Chandan Srivastava and Dr. Rekha M. of the Indian Institute of Science, Bangalore, for help with obtaining TEM micrographs and their interpretation.

REFERENCES

1. H.B. Huntington and A.R. Grone, *J. Phys. Chem. Solids* 20, 76 (1961).
2. J.R. Black, *IEEE Trans. Electron. Dev.* 16, 338 (1969).
3. C.K. Hu, R. Rosenberg, and K.Y. Lee, *Appl. Phys. Lett.* 74, 2945 (1999).

4. K.N. Tu, *J. Appl. Phys.* 94, 5451 (2003).
5. C.M. Tan, G. Zhang, and Z. Gan, *IEEE Trans. Dev. Mater. Reliab.* 4, 450 (2004).
6. I. Dutta, P. Kumar, and M.S. Bakir, *JOM* 63, 70 (2011).
7. J.W. Nah, J.O. Suh, and K.N. Tu, *J. Appl. Phys.* 98, 013715 (2005).
8. Y.-L. Shen, *J. Vac. Sci. Technol. B* 17, 2115 (1999).
9. H.V. Nguyen, C. Salm, B. Krabbenborg, K. Weide-Zaage, J. Bisschop, A.J. Mouthaan, and F.G. Kuper, *IEEE Annual International Reliability Physics Symposium* (2004).
10. C.J. Meechan and G.W. Lehman, *J. Appl. Phys.* 33, 634 (1962).
11. C. Chen, H.-Y. Hsiao, Y.-W. Chang, F. Ouyang, and K.N. Tu, *Mater. Sci. Eng. R* 73, 85 (2012).
12. G.J. van Gurp, P.J. de Waard, and F.J. du Chatenier, *Appl. Phys. Lett.* 45, 1054 (1984).
13. A.T. Huang, A.M. Gusak, K.N. Tu, and Y.S. Lai, *Appl. Phys. Lett.* 88, 141911 (2006).
14. N. Somaiah, D. Sharma, and P. Kumar, *J. Phys. D: Appl. Phys.* 49, 20LT01 (2016).
15. N. Somaiah and P. Kumar, *J. Appl. Phys.* 124, 185102 (2018).
16. N. Somaiah and P. Kumar, *Phys. Rev. Appl.* 10, 054052 (2018).
17. N. Somaiah and P. Kumar, *Nanotechnology*. https://doi.org/10.1088/1361-6528/ab3d5c. **(in Press)**.
18. I.A. Blech, *J. Appl. Phys.* 47, 1203 (1976).
19. D. Choi, C.S. Kim, D. Naveh, S. Chung, A.P. Warren, N.T. Nuhfer, M.F. Toney, K.R. Coffey, and K. Barmak, *Phys. Rev. B* 86, 045432 (2012).
20. W. Steinhogl, G. Schindler, G. Steinlesberger, and M. Englehardt, *Phys. Rev. B* 66, 075414 (2002).
21. I.A. Blech and C. Herring, *Appl. Phys. Lett.* 29, 131 (1976).
22. I.A. Blech and K.L. Tai, *Appl. Phys. Lett.* 30, 387 (1977).
23. I.A. Blech, *Acta Mater.* 46, 3717 (1998).

Publisher's Note Springer Nature remains neutral with regard to jurisdictional claims in published maps and institutional affiliations.